

## LEED AND AES STUDY OF THE Au/AuPb<sub>2</sub> INTERFACE

Jean-Paul BIBERIAN

*Laboratoire de Métallurgie et Physico-chimie des Surfaces, Université Pierre et Marie Curie, 11, rue Pierre et Marie Curie, 75231 Paris Cédex 05, France*

and

*Centre des Mécanismes de la Croissance Cristalline, UER Scientifique de Luminy, 70, route Léon Lachamp, 13288 Marseille Cédex 2, France*

Received 23 September 1977; manuscript received in final form 6 December 1977

The adsorption of lead on gold at room temperature in UHV conditions has been studied by LEED and AES. We review some of the data obtained on the Au(100), (111), and (110) faces, published elsewhere, and we give some new experimental results on the stepped Au(S) [ $n(100) \times (111)$ ] (with  $n = 3, 4, 5,$  and  $6$ ) faces. On all these faces, as lead is deposited on the gold substrate it first forms a monolayer of lead, then a compound AuPb<sub>2</sub>. Using the LEED and Auger data we give a model of the epitaxy with a layer-by-layer growth mechanism. We propose a model which involves a transition alloy which forms at the interface Au/AuPb<sub>2</sub>. This model is in agreement with the LEED diagrams observed before the one corresponding to bulk AuPb<sub>2</sub>. In the case of the epitaxy of lead on gold (100), we calculate the Auger peak-to-peak heights of the gold (72 eV) and lead (93 eV) transitions versus coverage. We obtain good agreement with the experimental data, assuming that the first and last layers of the alloy are lead monolayers and diffusion of lead in gold as well as gold in lead.

### 1. Introduction

The adsorption of lead on gold has been studied by various techniques. Schopper [1] and Weaver and Brown [2] used optical reflection, Snyman and Boswell [3] electron diffraction, Biberian et al. [4] and Perdereau et al. [5] LEED and AES. Pariset and Chauvineau [6] and Pariset et al. [7] used thin film conductivity and X-ray diffraction to examine alloyed layers.

All these experiments show that as the deposition of lead increases, there first forms a monolayer of lead, and then an intermetallic compound which has been identified as AuPb<sub>2</sub> between  $-150^{\circ}\text{C}$  and  $85^{\circ}\text{C}$ , and as Au<sub>2</sub>Pb above  $150^{\circ}\text{C}$ . These observations have been made on polycrystalline (111) oriented thin films, by electron and X-ray diffraction [3,7]. Biberian et al. [4] and Perdereau et al. [5] have observed the formation of the same compound on all the three faces, (100), (111), and (110), by LEED and AES.

Only surface sensitive techniques such as LEED and AES have been able to give

information on the structure of submonolayer quantities of lead. The results were first explained using a model of compact adsorbed layers [4,5] on (100), (111), and (110) faces. Recently, Biberian and Huber [8] have given a new description of the various structures of submonolayers on the (100) face.

We present here more detailed LEED and AES results for the (100), (111), and (110) faces, and some results for vicinal faces. A model is presented of the epitaxy of the AuPb<sub>2</sub> alloy on the (100), (111), and (110) faces, and a model is used to interpret the plot of Auger peak heights as a function of coverage.

## 2. Experimental method

The experimental apparatus and techniques are described by Biberian and Rhead [4]; we recall here the main experimental details. Experiments are performed in a Varian LEED chamber. Auger spectra are obtained by using the LEED gun as primary electron source, with an energy of 550 eV. Residual gas pressure is less than  $10^{-9}$  Torr. The specimen is mounted on a precision manipulator with micrometer displacements, and both the lead and gold are 99.999% pure. The lead is evaporated from a crucible heated at around 600°C and placed at 15 cm from the gold crystal. Deposition can be interrupted by turning the crystal and by rotating a cover over the lead source. The depositions are made with the substrate at room temperature. At the end of the run the surface is cleaned by argon ion bombardment.

In order to compare the three low Miller index faces (100), (111), and (110), the three single crystals were mounted on the same manipulator [5], and lead was deposited on the three faces simultaneously.

The four stepped surfaces plus a (100) surface were cut on the same single crystal, enabling us to compare them in the same conditions of cleaning of the crystal and deposition of lead.

## 3. LEED observations

### 3.1. Low-index faces

The LEED patterns have been described elsewhere [4,5]. The structures obtained for different times of deposition of lead (the substrate being at room temperature) are recalled in table 1.

If we compare table 1 with the results given in ref. [5], there are a few differences: on the (100) face, the structure  $c(6 \times 2)$  was first interpreted as a  $c(6 \times 6)$  structure with extinctions in the diffraction pattern, but all attempts to explain the extinctions by a double diffraction process have failed it seems more probably that the true structure is  $c(6 \times 2)$ , and the real space model for this is given in ref. [8]. On the (111) face, structure A was interpreted as a  $p(\sqrt{3} \times \sqrt{3})30^\circ$  structure. In

**Table 1**

Various structures observed on the (100), (111), and (110) faces of gold, during the deposition of lead at room temperature; see text for details

Evaporation time	(100) face	(111) face	(110) face
0	p( $\sim 5 \times \sim 20$ )	p( $\sim 20 \times \sim 20$ )	p(1 × 2)
0.25		p(1 × 1)	p(1 × 3)
0.37	p(1 × 1)	Structure A	
0.62	c(2 × 2)		p(1 × 1)
0.75	c( $7\sqrt{2} \times \sqrt{2}$ )45°	Structure B	p(7 × 1)
0.87	c( $3\sqrt{2} \times \sqrt{2}$ )45°		
1	c(6 × 2)		p(7 × 3)
1.12			p(4 × 4)
1.5	Structure H, 2 domains	Structure H, 1 domain	Structure H, 2 domains
2.0		Structure H, 2 domains	

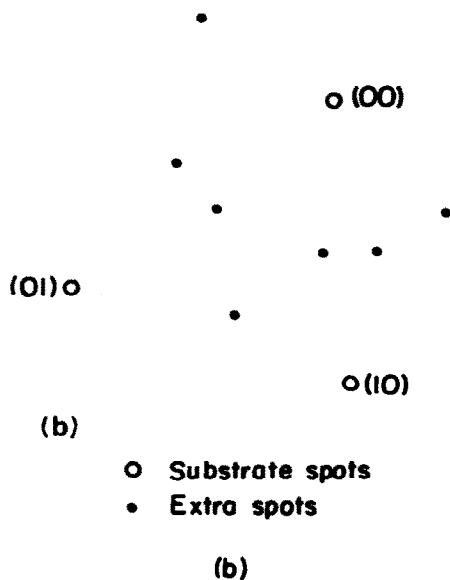
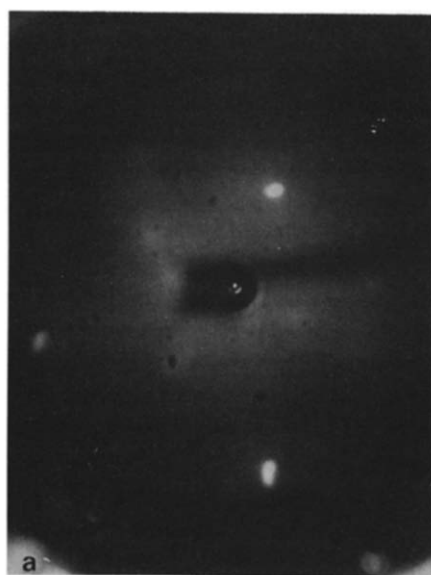


**Fig. 1.** Structure A. LEED pattern corresponding to the deposition of a submonolayer of lead on gold (111). The extra spots are weak and fuzzy, and this structure exists only in a very narrow coverage.

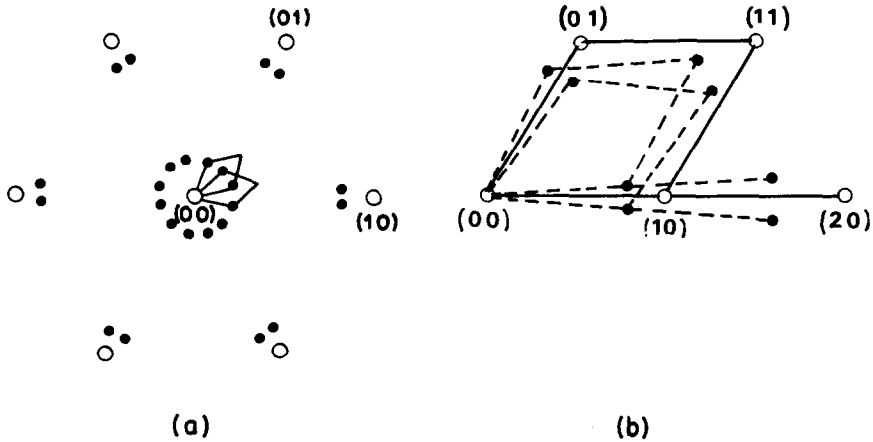


Fig. 2. Structure B. LEED pattern corresponding to the deposition of a monolayer of lead on gold (111). (a) LEED pattern showing six pairs of spots around each substrate spot. We have represented the small reciprocal unit mesh, with two domains, which had been previously chosen (see ref. [5]); (b) LEED pattern showing the extra spots around the (11) and (20) spots. This explains that the coincidence unit mesh is the one represented in dashed lines with two domains. The spots around the (00) beam are due to a double diffraction.

fact, more detailed observations have shown that we have a pattern as shown in fig. 1. Structure A never appears well resolved, but the pattern is significantly different from  $p(\sqrt{3} \times \sqrt{3})30^\circ$ . Structure B has been interpreted earlier with a small reciprocal unit mesh with extinctions [5]. The only extra spots of structure B are twelve satellite spots around the substrate spots (see fig. 2). So in the first interpretation [5], the coincidence unit mesh has been chosen as shown on fig. 2a, supposing that only the first order multiple diffraction beams are visible. An examination of the satellite spots around (11) and (20) beams shows the arrangement of fig. 2b: the satellite spots around them are not at the same distance as those around the (10) beams. So the diffraction patterns can be explained by a hexagonal overlay with two domains rotated of  $\pm 5^\circ$  from the substrate. The ratio of the atomic diameters of lead and gold in this arrangement is 1.15, compared with 1.21 for bulk crystals. The twelve spots around the (00) beam are due to double diffraction. Similarly, part of this ring is visible around the (10) beams. As the first domain of structure H appears, the doublets become faint, fuzzy, and unresolved. In some experiments another extra spot appears inside the doublet; this is probably the same hexagonal coincidence mesh, but non rotated.

### 3.2. Vicinal faces

We have studied 4 stepped surfaces close to the (100) face: (511), (711), (911) and (11, 1, 1). All of them were cut on the same crystal. These faces have (100) terraces of various width. We can denote them according to the notation of Lang et

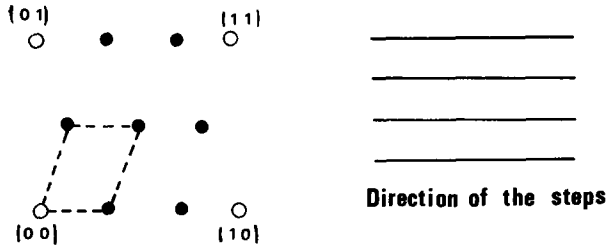


Fig. 3. Leed pattern corresponding to a  $c(6 \times 2)$  structure observed on  $[n(100) \times (111)]$  stepped surfaces, and corresponding to the deposition of a monolayer of lead. We have observed one domain for  $n = 3$  and 4, and two domains for  $n = 5$  and 6.

al. [9] as:  $[3(100) \times (111)]$ ,  $[4(100) \times (111)]$ ,  $[5(100) \times (111)]$  and  $[6(100) \times (111)]$  respectively.

When the crystal is clean, one observes the typical ( $\sim 5 \times \sim 20$ ) type pattern, but with only one orientation. As the deposition of lead increases, a  $(1 \times 1)$  structure appears, but with a splitting of certain reflexions as expected for stepped surface [10]. As the deposition increases, there occurs for the stepped surfaces patterns similar to the  $c(2 \times 2)$ ,  $c(7\sqrt{2} \times \sqrt{2})45^\circ$ , and  $c(3\sqrt{2} \times \sqrt{2})45^\circ$  patterns observed on the (100) face, but with splitting of reflexions that make the patterns very complex and difficult to interpret. When the coverage corresponds to a monolayer of lead, one observes a  $c(6 \times 2)$  structure, but with only one domain for the (511) and (711) faces, and two domains for the (911) and (11, 1, 1) faces (see fig. 3). When structure H appears on the (100) face, one observes only a single hexagonal domain on the four vicinal faces (see fig. 4).

#### 4. AES measurements

Biberian et al. [4] and Perdereau et al. [5] have given the variation of the peak-to-peak height of the Auger signals of gold (72 eV) and lead (93 eV) as a function

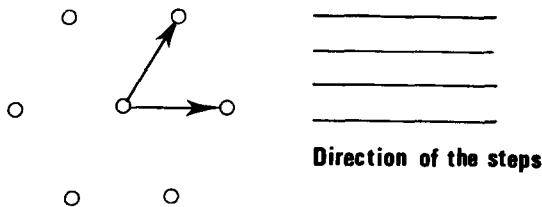


Fig. 4. Structure H observed on stepped  $[n(100) \times (111)]$  surfaces ( $n = 3, 4, 5,$  and 6) with one domain for all the faces.

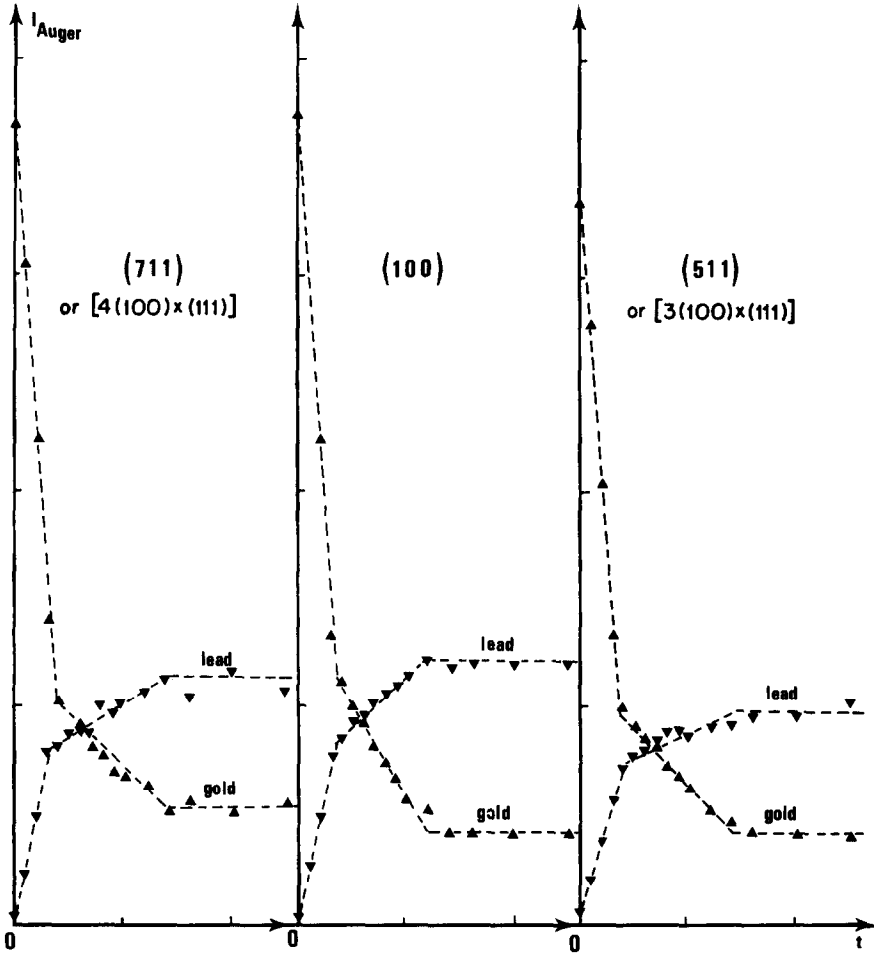


Fig. 5. Variation of the peak-to-peak height of the Auger signal for lead (93 eV) and gold (72 eV) versus the deposition time for the (100) face and two vicinal faces.

of coverage during lead deposition onto (100), (111), and (110) gold faces. Fig. 5 shows the plots for the (100) face, and the two vicinal faces (711) and (511). One can see that these curves, obtained simultaneously (the three faces being cut on the same crystal), are similar. The first "knees" in the plots of the three signals correspond to the completion of the monolayer of lead; they appear at the same deposition time for each face.

**5. Interpretation of the LEED and AES observations**

Perdereau et al. [5] have shown that for the three faces (100), (111), and (110) there first forms a monolayer of lead, then an alloy (the Auger signal of gold goes to a constant non-zero value at high lead coverages). This alloy has been identified by Snyman and Boswell [3] by electron diffraction, and by Pariset et al. [7] by X-ray diffraction as the intermetallic compound AuPb<sub>2</sub>. This compound is such that the (110) plane of AuPb<sub>2</sub> is parallel to the substrate plane for each of the three substrate orientations. Fig. 6 gives a projection of the AuPb<sub>2</sub> structure onto its (110) plane. One can see that the lead atoms labelled B and C or B' and C' form a pseudohexagonal monolayer. B atoms and C atoms (or B' and C') are not in the same plane; the distance between the planes is 1.66 Å.

It is important to understand, first, the structure of the monolayer of lead adsorbed on all the faces and, secondly, the epitaxy of AuPb<sub>2</sub>. We do not expect to find a model of the alloying mechanism, that is, to explain the diffusion mechanism which allows the gold atoms to diffuse into the adsorbed lead layer to form AuPb<sub>2</sub>. Oudar and Huber [11] have given a description of the epitaxy of AuPb<sub>2</sub> on the (110) face of gold for one orientation of AuPb<sub>2</sub> rectangular mesh. They are able to give a model of a possible mechanism to extract gold atoms from the substrate by a cooperative process. Here we give static models of epitaxy which are in agreement with the observed diffraction patterns, and with the AES measurements.

To interpret the structure of the monolayer of lead, we use, when possible, the high-symmetry model described by Huber and Oudar [12] and the more traditional compact model in the other cases.

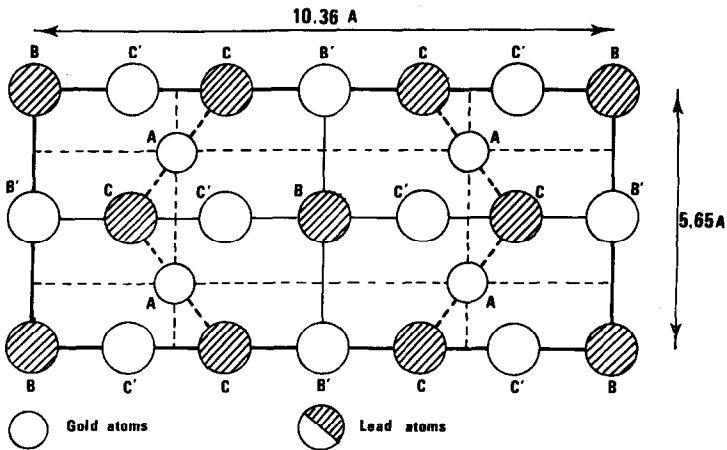


Fig. 6. A projection of the AuPb<sub>2</sub> compound on the (110) plane. The structure is generated by the stacking sequence ABCBA B'C'B'ABC... of the atomic layers.



model obtained assuming high symmetry of the coincidence mesh and that obtained supposing adsorption of a compact hexagonal monolayer close to a bulk plane are identical.

### 5.1.2. The epitaxy of AuPb<sub>2</sub>

Perdereau et al. [5] have shown that the unit mesh of the structure H does not coincide with the substrate (see figs. 8a and 8b). This often happens when a layer with hexagonal symmetry is adsorbed on a substrate with square symmetry.

The square surface unit mesh of Au(100) has sides of 2.88 Å, and the AuPb<sub>2</sub>

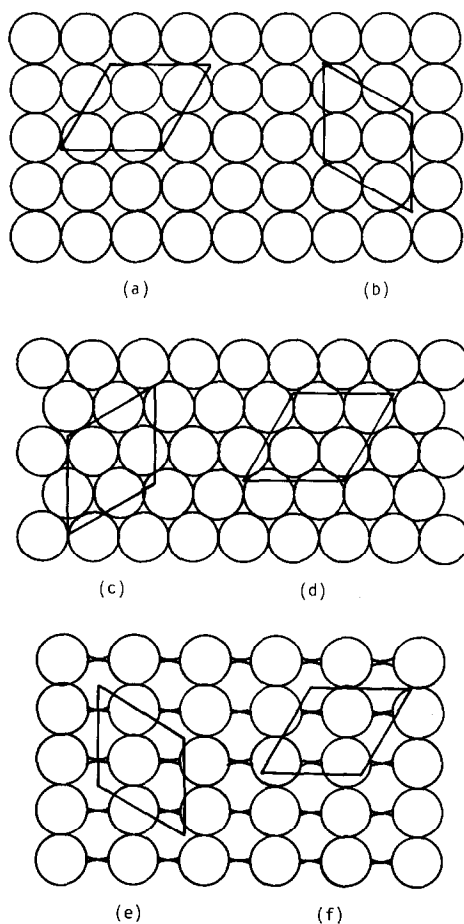


Fig. 8. A direct representation of the pseudohexagonal unit cell of AuPb<sub>2</sub>((100) plane) on the different faces of the gold substrate. (a) and (b) on the (100) face are equivalent; (c) and (d) on the (111) face and (e) and (f) on the (110) face are not equivalent.

alloy has a rectangular mesh with sides 5.65 and 10.36 Å. The double of the side of the gold mesh is equal to the width of the AuPb<sub>2</sub> rectangular mesh, within 2%. One can consider that there is coincidence in that direction. In the other direction, 5 times the length of AuPb<sub>2</sub> mesh (51.80 Å) is close to 18 times the side of the gold (100) square mesh (51.84 Å). So we can limit our study of the epitaxy to a (18 × 2) mesh.

In fig. 9a we have represented the lead atoms of the c(6 × 2) monolayer. In fact, we can consider the (18 × 2) mesh as composed of three c(6 × 2) meshes. In fig. 9b we have the same arrangement of lead atoms, but we have divided the (18 × 2) mesh into five AuPb<sub>2</sub> meshes. We can consider the lead atoms as being of the types B and C shown in fig. 6. The five meshes are not identical, and even in the same mesh B atoms (or C atoms) are not at equivalent positions. When the deposition of lead increases, the alloy grows by diffusion of gold from the substrate through the monolayer of lead. We shall examine this point in more detail in section 6.

With this model we interpret the c(6 × 2) monolayer of lead as being part of the alloy. When the deposition of lead increases, and the alloy grows, the symmetry which was imposed by the substrate by giving the c(6 × 2) structure is now imposed by the alloy, and leads to structure H. It is difficult to evaluate how much the lead atoms of the first layer move from their initial position in the Z direction, as the deposition of lead increases, but it is almost certain that they move since the lead atoms are now covered with a more or less thick layer of AuPb<sub>2</sub>. The interface between the gold substrate and the AuPb<sub>2</sub> thick layer is an intermediate alloy

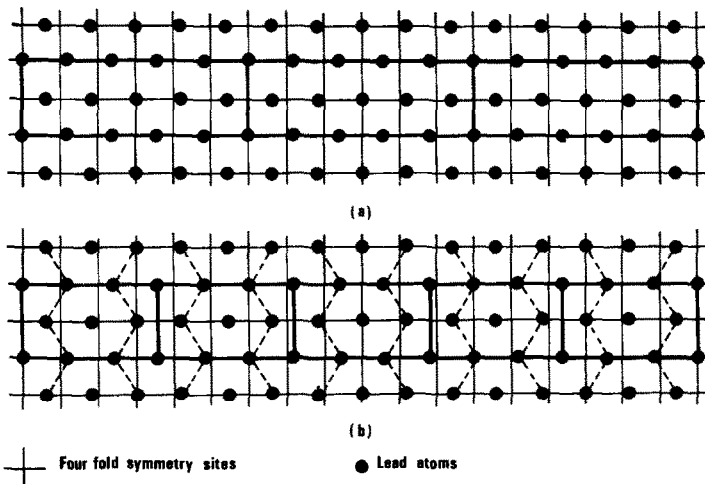


Fig. 9. (a) We have represented three c(6 × 2) unit cells of the lead monolayer forming a (18 × 2) cell. (b) The same lead atoms at the same positions, but this time we have divided the (18 × 2) cell into five AuPb<sub>2</sub> meshes. The lead atoms can now be considered as equivalent to the lead atoms B and C of fig. 6.

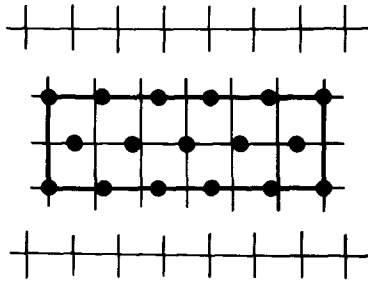


Fig. 10. Epitaxy of the  $c(6 \times 2)$  structure on a  $[4(100) \times (111)]$  face of gold.

which is neither a (111) plane of lead nor lead atoms in the position they should have in a perfect AuPb<sub>2</sub> compound. The important point is that the lead atoms of the first monolayer are in the right position according to their place in projection on the (110) plane of AuPb<sub>2</sub>. The only displacements required are in the Z direction to fit with the bulk AuPb<sub>2</sub>, and it is not necessary to assume the creation of dislocation or any other defect in the crystal during growth.

*5.2. The vicinal faces*

Vicinal faces are of great interest in the understanding of epitaxy, because the symmetry of the surface is broken on one direction. In fact, in the case of  $(n(100) \times (111))$  faces, we find an epitaxy equivalent to the adsorption of lead on the (100) surface, but in strips  $n$  atoms wide.

Fig. 10 shows the epitaxy of a  $c(6 \times 2)$  monolayer of lead on the  $(4(100) \times (111))$  face. If  $n$  is small (3 or 4), the terraces are not wide enough to allow the epitaxy of the  $c(2 \times 6)$  structure (perpendicular to the  $c(6 \times 2)$  structure), but if  $n$  is large enough (5 or 6), this epitaxy is possible. However, the diffraction patterns are not very intense.

Fig. 11 shows the epitaxy of AuPb<sub>2</sub> on the  $(4(100) \times (111))$  surface. In this case

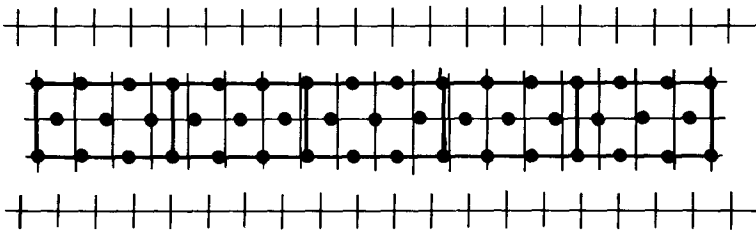


Fig. 11. We have represented the epitaxy of AuPb<sub>2</sub> on a  $[4(100) \times (111)]$  surface equivalent to the epitaxy on the (100) face shown in fig. 9.

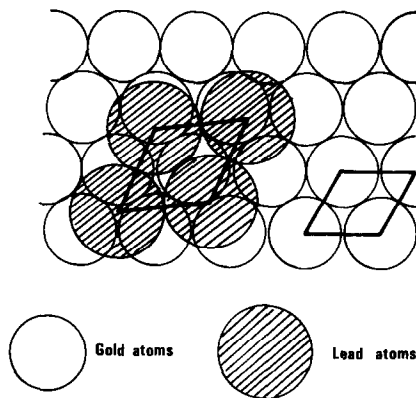


Fig. 12. Orientations of the compact layer of lead on the (111) face of gold. The two hexagonal unit meshes are rotated 5°.

too the epitaxy is possible but only in one direction, because even for the  $(6(100) \times (111))$  surface the terraces are not wide enough to allow the  $(18 \times 2)$  mesh to fit perpendicularly to the steps. This agrees with the experimental observations which show only one orientation for structure H for the four vicinal faces studied.

### 5.3. The (111) face

#### 5.3.1. Adsorption of a lead monolayer

As mentioned in section 3.1, during the formation of the lead monolayer a structure appears that is difficult to observe and to interpret (see fig. 1).

When the monolayer is completed, we observe structure B (see table 1) and the direct lattice deduced from the extra diffraction spots shows a hexagonal arrangement with a unit mesh close to that of the bulk (111) plane of lead. Fig. 12 shows that there is no coincidence mesh between the lead layer and the gold substrate. This is a case where the high symmetry model is not valid and an explanation of the diffraction pattern by adsorption of a compact hexagonal monolayer is more simple.

#### 5.3.2. The epitaxy of AuPb<sub>2</sub>

From table 1 we see that there appears first one domain of hexagonal structure, and then, as the deposition of lead increases, the second orientation appears. Fig. 8 gives the two direct unit meshes: (c) corresponds to the first orientation and (d) to the second. It is very surprising that orientation (d) appears later, because there is perfect coincidence with the substrate – we have in fact a  $p(2 \times 2)$  structure.

To clarify this point we have to look at the intermediate structure between structure B and structure H. We have seen in section 3.1 that, experimentally, as the

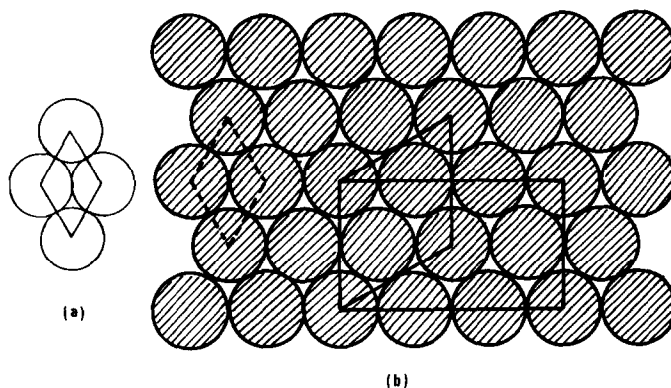


Fig. 13. (a) The gold (111) substrate. (b) The (111) plane of lead at the time of the growth of the AuPb<sub>2</sub> compound. The two hexagonal unit meshes of lead and gold are now parallel.

first domain of structure H appears, the doublets of the lead monolayer become faint, fuzzy, and unresolved: there appears to be a reorganisation of the lead monolayer, and the hexagonal unit mesh of the adsorbate becomes parallel to the gold unit mesh. So, in the same way as for the (100) face of gold, the reoriented hexagonal layer of lead is the first step of the growth of AuPb<sub>2</sub>. As shown in fig. 13, a (111) plane of lead can be considered as a part of the AuPb<sub>2</sub> alloy. The lead atoms correspond to B and C types of atoms of AuPb<sub>2</sub> described in fig. 6. The same discussion about the 2 positions of the lead atoms for the (100) face (see the end of section 5.2.1) is valid here.

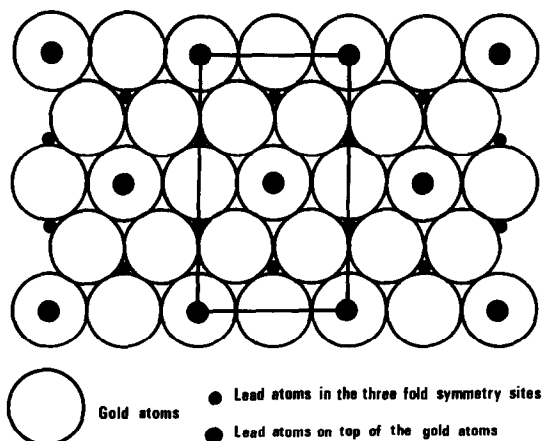


Fig. 14. We have represented the second orientation of AuPb<sub>2</sub> on the (111) face of gold. There are two kinds of lead atoms: those in the three fold symmetry site, and those on top of the gold atoms. They are equivalent to the C and B atoms of figure 6 respectively.

The second orientation (fig. 8d) appears afterwards. Two hypotheses are possible: first, this orientation is produced by faults during the formation of the early arrangement; secondly, this orientation appears by direct epitaxy on the gold substrate. As shown in fig. 14, there are two kinds of lead atoms: the B type atoms (fig. 6) are on top of the gold atoms and the C type atoms are in the three fold symmetry sites. The lead atoms of fig. 14 form a hexagonal layer, but rotated of 30° with respect to the lead layer of fig. 13; explaining the first orientation. So this second hypothesis supposes a rotation of 30° of the lead monolayer. It is difficult to choose between the two hypotheses.

#### 5.4. The (110) face

##### 5.4.1. Adsorption of a lead monolayer

In a previous paper [5] Perdereau et al. have described the  $p(7 \times 1)$ ,  $p(7 \times 3)$  and  $p(4 \times 4)$  structures that occur during the deposition onto the (110) face. Recently Oudar and Huber [11] have given a model of one of the oblique epitaxies of AuPb<sub>2</sub> on the (110) face in which the  $p(7 \times 3)$  and  $p(4 \times 4)$  structures are considered as structures of a transitional alloy. Therefore, the only structure that would correspond to a simple lead monolayer is the  $p(7 \times 1)$  structure. A simple model consists of six lead atoms for seven sites in the gold rows of the surface [5].

##### 5.4.2. The epitaxy of AuPb<sub>2</sub>

Figs. 8e and 8f show the two orientations of the AuPb<sub>2</sub> pseudo-hexagonal unit

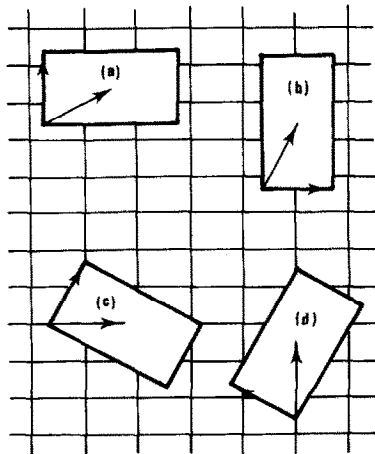


Fig. 15. The four orientations of the AuPb<sub>2</sub> rectangular mesh on the (110) face of gold.

mesh on the (110) gold surface, and fig. 15 shows the four orientations of the AuPb<sub>2</sub> rectangular unit mesh. Orientation (e) of fig. 8 corresponds to (a) and (d) of fig. 15, and orientation f of fig. 8 to (b) and (c) of fig. 15.

Oudar and Huber [11] have given an interpretation corresponding to the epitaxy of fig. 15 (d), and they give a model with a very large coincidence mesh. In fact, they suppose that this mesh is not observed, but that it is broken into smaller meshes that correspond to the  $p(7 \times 3)$  and  $p(4 \times 4)$  observed structures. We shall give here interpretation for the three other possible orientations. Some of the models lead to structures corresponding to observed patterns, and they therefore can be considered as realistic. Some models do not, but we give them to show the different steps of the method and its limits.

*5.4.2.1. Epitaxy corresponding to the orientation of fig. 15a.* If we try to fit AuPb<sub>2</sub> on the (110) gold substrate, we see that there is no possible direct epitaxy. Fig. 16a shows a possible epitaxy but with a 20% dilatation, and a  $p(2 \times 3)$  surstructure. Fig. 16b gives a model with a 20% contraction and a  $p(2 \times 2)$  surstructure, and fig. 16c, obtained by an association of the two other models, has a 2% difference and a  $p(2 \times 5)$  surstructure. But neither of these structures has been observed.

*5.4.2.2. Epitaxy corresponding to the orientation of fig. 15b.* Fig. 17a shows a model for this epitaxy. In this case the alloy is dilated by 11% in length and contracted 4% in width. The coincidence mesh is  $c(4 \times 4)$ . Such an arrangement is possible only when this layer is stabilized by a thicker layer of alloy, because the lead atoms are not in stable positions as explained at the beginning of section 5. In the first stages of formation of the alloy the atomic arrangement might be quite different. Fig. 17b shows a possible position of the lead atoms after a relaxation of the

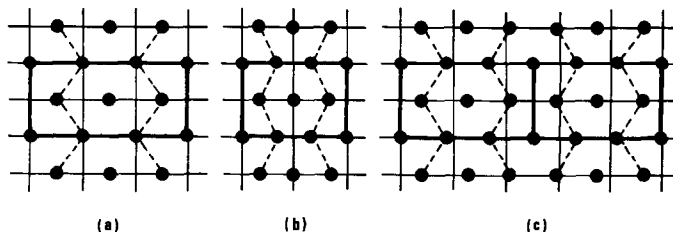


Fig. 16. Epitaxy corresponding to fig. 15a. (a), (b), and (c) represent attempts to coincide the AuPb<sub>2</sub> mesh with the (110) substrate by distorting the compound, but none of the resulting coincidence meshes are observed. The black circles represent the centers of the lead atoms, and the intersections of the lines, the four fold coordination sites.

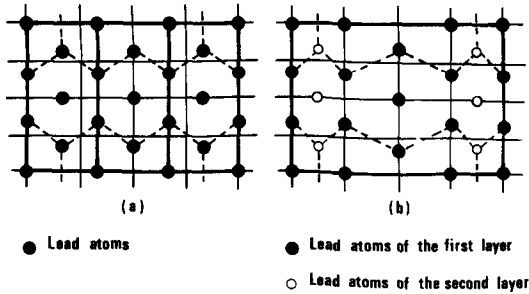


Fig. 17. Epitaxy corresponding to fig 15b. (a) A very small distortion in the dimensions of the AuPb<sub>2</sub> unit mesh permits a coincidence of three AuPb<sub>2</sub> rectangular meshes with sixteen unit meshes of the substrate. This corresponds to a  $c(4 \times 4)$  coincidence mesh which is not observed. (b) Same epitaxy as in (a), but we have relaxed the lead atoms so that they go in the rows formed by the gold atoms of the (110) surface, and then in the rows formed by the lead atoms themselves. This correspond to a  $p(4 \times 4)$  coincidence mesh which was observed experimentally.

layer. We see that there are two types of lead atoms: some are in the rows of the gold substrate and correspond approximatively to the first layer of lead, and some are in the sites formed by the lead atoms of the first layer. All the rows of the gold surface are filled (three atoms of lead for four sites) and half of the rows formed by the first layer of lead are filled by lead atoms of the second layer. The coincidence mesh is  $p(4 \times 4)$  and not  $c(4 \times 4)$  as before. The corresponding observed pattern is not very well defined: the spots of the  $(x, n/4)$  type (with  $n = 1, 2, 3$ ) are not resolved, and streaks appear [5]. These are probably due to the fact that the lead atoms are not well ordered because of a lack of interaction between the lead atoms of the different rows.

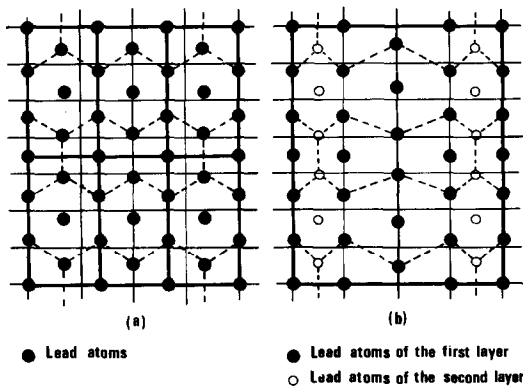


Fig. 18. Epitaxy corresponding to fig. 15b. Same legend as for fig. 17. Here the AuPb<sub>2</sub> mesh is less distorted, but the resulting  $p(7 \times 4)$  coincidence mesh is not observed experimentally.

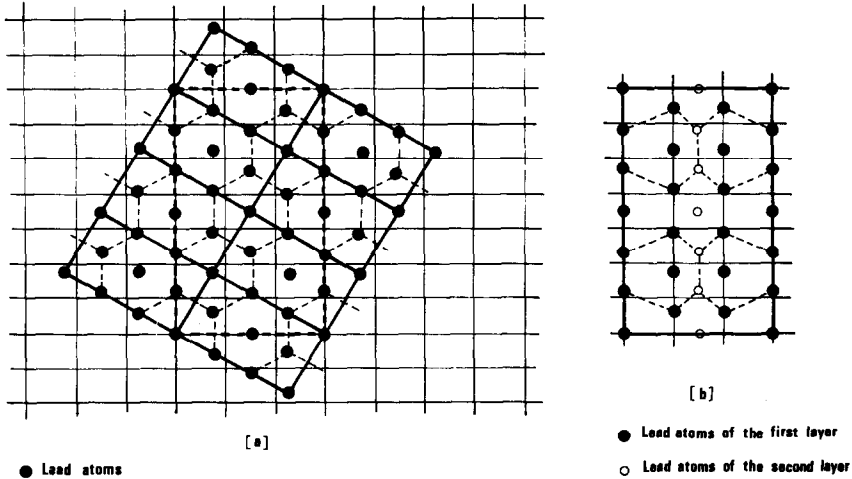


Fig. 19. Epitaxy corresponding to fig. 15c. Same legend as for fig. 17, but here the  $p(7 \times 3)$  coincidence mesh is observed.

Another possible epitaxy is shown in fig. 18a. Here the coincidence mesh is  $p(7 \times 4)$  and the alloy is contracted by 2.5% in length and 4% in width. Fig. 18b shows the atomic positions when the layer is not stabilized by a thicker layer of alloy. The lead atoms of the first layer are those of the  $p(7 \times 1)$  structure, and those of the second layer are in the sites of the first layer. A  $p(7 \times 4)$  structure is not observed experimentally.

*5.4.2.3. Epitaxy corresponding to the orientation of fig. 15c.* Fig. 19a shows a model for this epitaxy, the AuPb<sub>2</sub> rectangular mesh is dilated by 1% in length and 6% in width, and the mesh is not perfectly rectangular, the angle being  $88^\circ$ . Just as in section 5.4.2.2, a relaxation of the lead atoms give the model of fig. 19b. Here too we see that the lead atoms of the first layer are those of the  $p(7 \times 1)$  structure and those of the second layer are in the sites of the first layer. As for the  $p(4 \times 4)$  structure, the lack of interaction between the lead atoms would explain the streaks of the diffraction patterns [5].

We conclude therefore that the models of figs. 17 and 19 explain the experimental observations of the  $p(4 \times 4)$  and  $p(7 \times 3)$  structures.

## 6. Study of the Auger spectra for the (100) face

The variation of the peak-to-peak height of the Auger spectrum versus coverage has been described for simple models during a layer-by-layer growth mechanism [12–14]. Recently, many authors have tried to apply simple models for the study

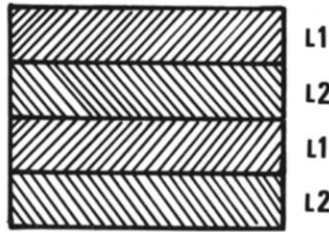


Fig. 20. This is a sketch of the three-dimensional AuPb<sub>2</sub>. We have divided the unit cell into two kinds of layers, L1 and L2. L1 is composed only of lead atoms, and L2 is composed of 2 atoms of gold for one atom of lead. See fig. 21 for details.

of the depth profiling of the alloys (see, for example, ref. [15]). All these models are based on a continuous variation of the concentration with depth, while here AuPb<sub>2</sub> has a layered structure (layers of lead and layers of compounds; see fig. 20). Here we give a model of the variation of the gold (72 eV) and lead (93 eV) Auger signals during the growth of very thin AuPb<sub>2</sub> film. We use the model described in section 5 for the formation of AuPb<sub>2</sub> on a (100) face of gold, and we show that the results are in agreement with the model proposed for the epitaxy in section 5. We do not try the same analysis on the (111) and (111) faces of gold, because as we have seen in section 5, the models of epitaxy for these two faces are uncertain, while on the (100) face the model is coherent from the beginning of the deposition of lead up to the formation of the alloy.

### 6.1. Theoretical formulation

We can consider the AuPb<sub>2</sub> alloy as formed of an alternation of two kinds of layers (see fig. 20), L1 and L2. L1 is composed of six atoms of lead per rectangular

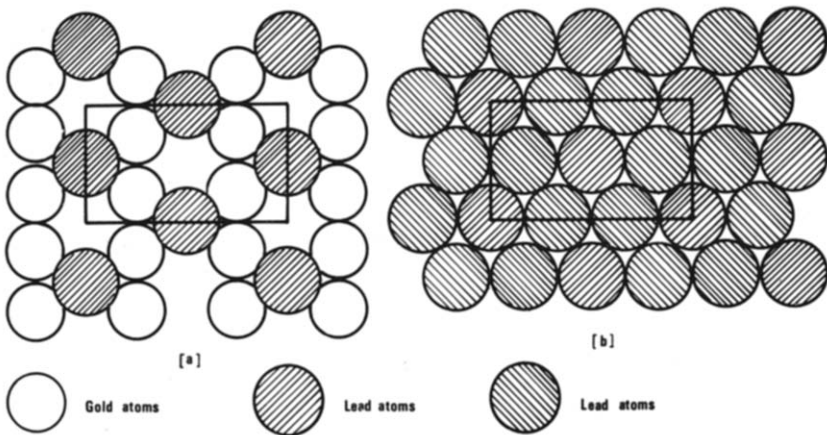


Fig. 21. (a) L2-type layer, composed of gold atoms (A type in fig. 6) and lead atoms (B' type in fig. 6). (b) L1-type layer, composed of lead atoms (B and C types in fig. 6).

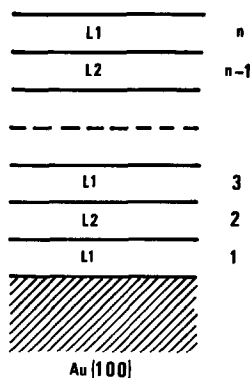


Fig. 22. Representation of  $n$  layers of L1 or L2 (a layer of AuPb<sub>2</sub> is formed of 4 of these layers, L1 + L2 + L1 + L2) on the (100) face of gold. We note that the first and the last layers are always of the L1 type, that is, a monolayer of lead. The growth is double layer (L2 + L1) by double layer on a monolayer (L1) of lead.

cell, and L2 is composed of two atoms of lead and four atoms of gold. L1 is formed by atoms of B and C types, and L2 is formed by atoms of B' and A types (see fig. 6). The L1 and L2 layers are described in fig. 21. The L1 type is approximately hexagonal.

At any time during the deposition of lead on gold (100) there is an increase of the gold Auger peak which could be due to a diffusion of gold on top of the lead or alloy layer. Thus we can suppose that during the growth the AuPb<sub>2</sub> alloy is always covered by a lead monolayer L1. So the model we adopt consists of a growth double layer by double layer (L1 + L2). We have deduced from the LEED observations (see section 5) that AuPb<sub>2</sub> grows from a lead monolayer (L1 type) adsorbed on gold (100). Fig. 22 gives a schematic view of the growth. So the number of complete adsorbed layers  $n$  is always odd.

In the appendix we calculate  $I_{Pb_n}$  and  $I_{Au_n}$ , the Auger signals relative to the lead (93 eV) and gold (72 eV) Auger peaks.

### 6.2. Comparison with the experimental curves

In fig. 23 we measure (in arbitrary units):  $I_{Au_0} = 196$ ,  $I_{Au_1} = 59$ ,  $I_{Au_\infty} = 21$ ,  $I_{Pb_1} = 41$ , and  $I_{Pb_\infty} = 60$ . This gives (see appendix), from eq. (10):  $\alpha_{Au} = 0.301$ ; and from eq. (11):  $I_{Au}^{L1+L2} = 19.1$ . By solving eq. (14), we obtain:  $\alpha_{Pb} = 0.46$ . Then from eq. (13) we deduce:  $I_{Pb}^{L1+L2} = 47.3$ .

With these values of the parameters we can calculate:  $I_{Pb_n}$  and  $I_{Au_n}$  from eqs. (5) and (6); with  $n = 3, 5, 7$ :  $I_{Pb_3} = 56.0$ ,  $I_{Pb_5} = 59.1$ ,  $I_{Pb_7} = 59.8$ ,  $I_{Au_3} = 24.5$ ,  $I_{Au_5} = 21.3$ ,  $I_{Au_7} = 21$ .

A first remark about the above results is that  $I_{Pb_7}$  and  $I_{Au_7}$  are practically equal to  $I_{Pb_\infty}$  and  $I_{Au_\infty}$  respectively. A second remark is that if we normalize the deposi-

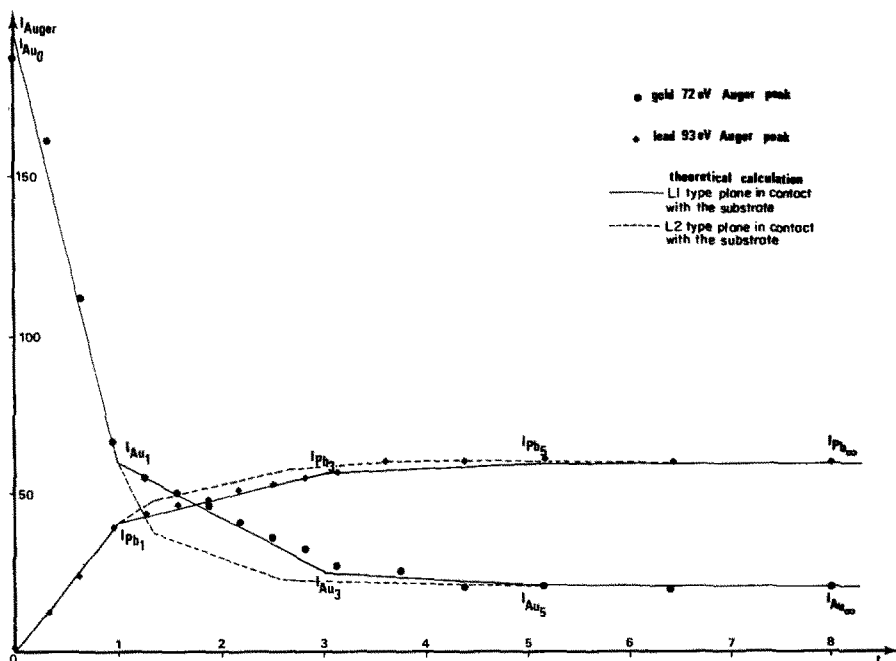


Fig. 23. Auger plot of the gold (72 eV) and lead (93 eV) peaks versus the deposition time of lead on gold (100). These curves are independent of the deposition rate in the range of one monolayer per minute to one monolayer per 30 minutes. For convenience we have normalized  $t = 1$  at the formation of the monolayer of lead (first break in both curves). We have compared two theoretical curves to the experimental points. See text for details.

tion time at  $t = 1$  for the formation of a monolayer, then we need a deposition time of  $t = 2.33$  to form L1 + L2 + L1, and  $t = 5.67$  to form L1 + L2 + L1 + L2 + L1, because an L2 layer contains only one third lead atoms. If we compare the values obtained for  $I_{Pb_3}$  and  $I_{Au_3}$  to the experimental curves, we see that at  $t = 2.33$  the difference is large, while at  $t = 3$  the calculated values are almost identical to the experimental one (see fig. 23).

This is an important point, because it shows that to form a L2 layer we need as many lead atoms as to form a L1 layer; that is to say, if gold diffuses in the lead layer, lead diffuses simultaneously in the gold substrate.

### 6.3. Discussion

We have developed an exact model to explain the experimental Auger curves. The agreement between experimental and theoretical values is very good. This is an a posteriori confirmation of the following hypotheses:

(1) First an adsorption of a lead monolayer, occurs then the adsorption of double

layers, with always a monolayer of lead at the top.

(2) The inelastic mean free path (imfp) for 72 and 93 eV electrons are the same in gold, lead, and the alloy, and the backscattering factor is constant.

(3) When the alloy is formed, as gold diffuses into the lead, lead diffuses into the gold.

We can deduce also that:  $\alpha_{Au} = 0.30$ ,  $\alpha_{Pb} = 0.46$ , or  $\lambda_{Au} = 1.4$  layer,  $\lambda_{Pb} = 1.7$  layer, or  $\lambda_{72eV} = 4.9$  Å,  $\lambda_{93eV} = 6$  Å.

The  $\lambda$ 's are the inelastic mean free paths for the 72 and 93 eV electrons in gold or lead.

The third hypothesis is needed because of the bad agreement between theoretical and experimental curves. Also one can ask if the model chosen is good, and whether another model cannot give a better fit.

First of all, we can suppose that the alloy is not AuPb<sub>2</sub>, but Au<sub>2</sub>Pb, as observed by Snyman and Boswell [3] and Pariset et al. [7] in some cases. The structure of Au<sub>2</sub>Pb is hexagonal on projection on the (111) plane, the side of the hexagonal unit mesh being 5.60 Å. So from the diffraction pattern it is impossible to distinguish between the two structures. But in bulk Au<sub>2</sub>Pb there is no dense plane of lead, and it is impossible to explain the value of the lead Auger peak without supposing a dense plane of lead on top of the alloy, since most of the Auger signal is given by the first layer at low electron energies (93 eV).

Another possibility is to have an epitaxy of AuPb<sub>2</sub> on the gold substrate through an L2-type layer. We have shown in fig. 23 the theoretical curves with and without diffusion of lead in the substrate, and in both cases the agreement is worse than in the model with epitaxy through an L1-type layer.

## Conclusion

We have shown in this study that LEED and AES are suitable tools for understanding the first steps of epitaxy, in the particular case of AuPb<sub>2</sub> growth on gold.

We have observed that on all the faces studied: (100), (111) and (110) and the stepped surfaces [ $n(100) \times (111)$ ] ( $n = 3, 4, 5, 6$ ), the same compound is formed during the evaporation of lead. The (110) plane of AuPb<sub>2</sub> is always parallel to the surface of the substrate. The model we have developed here shows that the atoms of the compound in contact with the substrate are always lead atoms forming a compact plane close to a (111) plane of bulk lead, except for the (110) face, where the lead atoms are in the rows formed by the gold atoms at the surface.

In the particular case of the growth of the AuPb<sub>2</sub> compound on the (100) face of gold, we have given a full description of all the steps of the epitaxy, from the submonolayer of lead to the formation of a thick layer of AuPb<sub>2</sub>. A model of the Auger intensities fits very well with the experiment, and shows that there is diffusion of lead in gold as well as diffusion of gold in lead. Also the Auger measurements show that the top layer of the alloy is always a lead monolayer.

The LEED observations of the stepped surfaces vicinal to the (100) plane are in agreement with the model of the epitaxy on the (100) face.

In the case of the epitaxy on the (111) face of gold, there are more uncertainties in the interpretation of the LEED structures. This is due to the fact that we have not found a satisfactory model for the epitaxy of the first monolayer of lead. Nevertheless, we have proposed a model for the epitaxy of AuPb<sub>2</sub>, in agreement with the LEED observations and the Auger data.

The epitaxy of AuPb<sub>2</sub> on the (110) face of gold is highly interesting, because of the intermediate structure observed by LEED during the alloying. These structures correspond to transition alloys at the interface at the time of the growth of the compound. We have proposed several models that agree with the observations, but should only be considered as such. The number of unknown parameters being large, it is hard to give a precise description.

We have shown that in some cases, where the adsorbate structure is known by other means (here X-ray [6,7] and electron [3] diffraction), it is possible to get more information from the LEED and Auger data, using adequate models.

## Appendix

Here we calculate  $I_{Pb_n}$  and  $I_{Au_n}$ , the Auger signals relative to the lead (93 eV) and gold (72 eV) Auger peaks. For these we need to know:

$I_{Pb_1}$ : the Auger signal of a monolayer of lead,

$I_{Pb}^{L1+L2}$ : the lead Auger signal of a double layer L1 + L2,

$I_{Au}^{L1+L2}$ : the gold Auger signal of a double layer L1 + L2,

$\lambda_{pb}$ : the inelastic mean free path of 93 eV Auger electrons,

$\lambda_{Au}$ : the inelastic mean free path of 72 eV Auger electrons (we suppose that  $\lambda_{pb}$  and  $\lambda_{Au}$  are independent of the material: lead, gold, or alloy, because the atomic numbers of lead and gold are very close).

$\lambda_{pb}$  and  $\lambda_{Au}$  are related to  $\alpha_{pb}$  and  $\alpha_{Au}$ , the attenuation factors by the formulae deduced from ref. [14]:

$$\alpha_{Au} = \exp(-1/0.74\lambda_{Au}), \quad \alpha_{pb} = \exp(-1/0.74\lambda_{pb}).$$

The 0.74 factor is due to geometrical considerations, and is valid for a grid Auger analyser and a CMA.

We can write:

$$I_{Pb_n} = \alpha_{pb}^{n-1} I_{Pb_1} + (1 + \alpha_{pb}^2 + \dots + \alpha_{pb}^{n-5} + \alpha_{pb}^{n-3}) I_{Pb}^{L1+L2}. \quad (1)$$

In the case of the gold Auger signal,  $I_{Au_n}$ , is composed of two parts:  $I'_{Au_n}$  is due to the gold present in the adsorbed alloy, and  $I''_{Au_n}$  to the substrate signal attenuated by the adsorbed alloy. So:

$$I_{Au_n} = I'_{Au_n} + I''_{Au_n}.$$

We can write, as for (1):

$$I'_{Au_n} = (1 + \alpha_{Au}^2 + \dots + \alpha_{Au}^{n-5} + \alpha_{Au}^{n-3}) I_{Au}^{L1+L2}, \quad (2)$$

$$I''_{Au_n} = \alpha_{Au}^n I_{Au_0}, \quad (3)$$

where  $I_{Au_0}$  is the gold Auger signal of the clean (100) surface. From (2) and (3), we deduce:

$$I_{Au_n} = \alpha_{Au}^n I_{Au_0} + (1 + \alpha_{Au}^2 + \dots + \alpha_{Au}^{n-5} + \alpha_{Au}^{n-3}) I_{Au}^{L1+L2}. \quad (4)$$

Relations (1) and (4) can be rewritten:

$$I_{Pb_n} = \alpha_{Pb}^{n-1} I_{Pb_1} + \frac{1 - \alpha_{Pb}^{n-1}}{1 - \alpha_{Pb}^2} I_{Pb}^{L1+L2}, \quad (5)$$

$$I_{Au_n} = \alpha_{Au}^n I_{Au_0} + \frac{1 - \alpha_{Au}^{n-1}}{1 - \alpha_{Au}^2} I_{Au}^{L1+L2}. \quad (6)$$

Relations (5) and (6) give for  $n = \infty$ :

$$I_{Pb_\infty} = \frac{1}{1 - \alpha_{Pb}^2} I_{Pb}^{L1+L2}, \quad (7)$$

$$I_{Au_\infty} = \frac{1}{1 - \alpha_{Au}^2} I_{Au}^{L1+L2}. \quad (8)$$

For  $n = 1$ , relation (6) gives:

$$I_{Au_1} = \alpha_{Au} I_{Au_0}. \quad (9)$$

We can easily measure on the experimental curves (see fig. 23):

$$I_{Au_0}, I_{Au_1}, I_{Au_\infty}, I_{Pb_1}, I_{Pb_\infty}.$$

From relation (9) we deduce:

$$\alpha_{Au} = I_{Au_1} / I_{Au_0}. \quad (10)$$

From relation (8) we deduce:

$$I_{Au}^{L1+L2} = (1 - \alpha_{Au}^2) I_{Au_\infty}, \quad (11)$$

or

$$I_{Au}^{L1+L2} = \left( 1 - \left( \frac{I_{Au_1}}{I_{Au_0}} \right)^2 \right) I_{Au_\infty}. \quad (12)$$

Relation (7) has two parameters:  $\alpha_{Pb}$  and  $I_{Pb}^{L1+L2}$ . We can calculate  $I_{Pb}^{L1+L2}$  by considering it as composed of a double layer L1 + L2. With this hypothesis  $I_{Pb}^{L1+L2}$  is the addition of the Auger signal of L1 layer and the lead Auger of a L2 layer (1/3 of L1 layer) attenuated by L1 layer. So:

$$I_{Pb}^{L1+L2} = I_{Pb_1} + \alpha_{Pb} I_{Pb_1} / 3, \quad (13)$$

From relations (7) and (13) we deduce:

$$I_{\text{Pb}\infty} = \frac{1 + \alpha_{\text{Pb}/3}}{1 - \alpha_{\text{Pb}}^2} I_{\text{Pb}1}. \quad (14)$$

This is a second-order equation in  $\alpha_{\text{Pb}}$  which has only one positive root.

## References

- [1] H. Schopper, *Z. Physik* 143 (1955) 93.
- [2] C. Weaver and L.C. Brown, *Phil. Mag.* 8 (1963) 1379.
- [3] H.C. Snyman and F.W. Boswell, *Surface Sci.* 41 (1974) 21.
- [4] J.P. Biberian and G.E. Rhead, *J. Phys. F (Metal Phys.)* 3 (1973) 675.
- [5] J. Perdereau, J.P. Biberian and G.E. Rhead, *J. Phys. F. (Metal Phys.)* 4 (1974) 798.
- [6] C. Pariset and J.P. Chavineau, *Surface Sci.* 47 (1975) 543.
- [7] C. Pariset, M. Galtier and M. Gasgnier, *Thin Solid Film* 29 (1975) 325.
- [8] J.P. Biberian and M. Huber, *Surface Sci.* 55 (1976) 259.
- [9] B. Lang, R.W. Joyner and G.A. Somorjai, *Surface Sci.* 30 (1972) 440.
- [10] G.E. Rhead and J. Perdereau, in: *Structure et Propriétés des Surfaces des Solides* (CNRS, Paris, 1969) p. 37.
- [11] J. Oudar and M. Huber, *J. Crystal Growth* 31 (1975) 345.
- [12] M. Huber and J. Oudar, *Surface Sci.* 47 (1975) 605.
- [13] T.E. Gallon, *Surface Sci.* 17 (1969) 486.
- [14] D.C. Jackson, T.E. Gallon and A. Chambers, *Surface Sci.* 36 (1973) 381.
- [15] M.P. Seah, *Surface Sci.* 32 (1972) 703.
- [16] C.C. Chang, *Surface Sci.* 48 (1975) 9.